Letters

Enhanced Frequency-Locked Loop With a Comb Filter Under Adverse Grid Conditions

Huawu Liu, Yan Xing, and Haibing Hu

***Abstract*—To improve the performance of frequency-locked loops (FLLs) under distorted grid conditions, the technique of harmonic decoupling with multiple notch filters was usually employed to remove the harmonic components, which, although offering good filtering abilities, suffers from complexity, high computational burden, and deteriorated dynamics. To alleviate these problems, this letter proposes an enhanced adaptive notch-filter-based FLL, which incorporates a comb filter and improves the filtering abilities by introducing purely imaginary zeros to achieve notch peaks and harmonic cancellation. In comparison with the typical existing solutions of multiple notch-filter-based FLLs for distorted grid systems, the proposed FLL features simple structure and low computational load, and it can completely block the dc component, odd and even harmonics of the input grid voltage without sacrificing the FLL dynamics. Experimental results and comparisons are presented to validate the effectiveness of the proposed FLL.**

***Index Terms*—Comb filter, frequency-locked loop, grid synchronization, harmonic rejection.**

I. Introduction

SYNCHRONIZATION is a key aspect for grid-connected converters. Among the various synchronization methods, closed-loop techniques, which can be mainly categorized into phase-locked loops (PLLs) and frequency-locked loops (FLLs), are probably the most widely used within the area of power electronic due to their simplicity, robustness, and effectiveness.

Conventional PLLs/FLLs usually exhibit unacceptable frequency and phase errors when the utility grid is distorted. Therefore, many improved PLLs/FLLs [1]–[19] have been proposed. The basic concept of these methods is to enhance the filtering ability by employing additional filters either in the control loop (called the in-loop filtering techniques) or before the input of the loop (called the prefiltering techniques). Typical prefiltering PLLs, such as multiple reference frame PLL [1], multiple complex-coefficient-filter-based PLL [2], PLL with decoupling network in the $\alpha\beta$-frame (DN$\alpha\beta$-PLL) [3], etc., rely on the technique of harmonic decoupling network [4]. Although harmonic rejection capabilities of these PLLs can be significantly improved, increased complexity and heavy computational burden is the major limitation [5]. Besides, the PLL dynamic response is also affected due to interactions between the filtering stage and PLL loop [6]. For in-loop filtering PLLs, the effective and low computational load filters are often applied, such as the MAF-PLL [7], [8], CDSC-PLL [9], [10], RPC-based PLL [11], etc. These filters essentially function as low-pass filters to extract dc component of the output of phase detector while attenuating the rest harmonics [10]. Yet, transient responses of the PLLs are sacrificed due to the introduced delay [7], and the literatures [12], [13] are further devoted to improve the PLL dynamics. An FLL locks the frequency of the grid voltage instead of the phase angle, and the phase angle is calculated outside the loop. Due to inherent differences between the FLL and PLL [7], where bandpass filtering characteristics are required to extract the fundamental components and attenuate/eliminate the other harmonics in the FLL system, the in-loop low-passing filters (MAF, CDSC filter, repetitive filter, etc.) [7]–[11] that are widely used in PLLs, cannot be directly applied to the FLLs. Therefore, in order to adapt FLLs for adverse grid systems, multiple preloop notch filters are often employed [5], [14]–[18]. These FLLs provide good filtering ability, but suffer from heavy computational burden [5].

In this letter, a comb filter is proposed to be incorporated into the conventional SOGI-FLL [18] to enhance its harmonic rejection ability. Detailed analysis of the proposed approach is provided, which shows that dc, odd and even harmonics of the grid voltage can be completely rejected, and fast dynamics of the original SOGI-FLL are also maintained. Experimental results are further given to validate the effectiveness of the proposed FLL.

II. Proposed FLL Under Distorted Grid Conditions

A. Conventional Adaptive Notch-Filter-Based FLL and Solutions for Distorted Grid Systems

Adaptive notch-filter-based FLL (ANF-FLL) is a powerful tool to estimate the amplitude, phase, and frequency of a periodic signal [14]–[18]. Among the various structures of ANF-FLL, SOGI-FLL [18] shown in Fig. 1 is a typical and widely researched one. The conventional SOGI-FLL can provide good accuracy and dynamics when the grid is clean. However, under distorted grid conditions, the synchronization errors become unacceptable because of the limited attenuation ability of the SOGI filter [19]. Fig. 2 illustrates its performance when the grid is distorted with 15% third harmonic. It can be seen that the frequency error is unacceptably large, i.e., around ± 1.8 Hz.

To enhance the filtering ability and improve the accuracy of the ANF-FLL under adverse grid conditions, existing solutions usually utilizes the multiharmonic decoupling network (MDN), which consists of multiple notch filters [2], [5], [14]–[16]. A

Manuscript received February 29, 2016; revised March 24, 2016 and April 25, 2016; accepted April 30, 2016. Date of publication May 09, 2016; date of current version July 08, 2016. This work was supported by the National Natural Science Foundation of China under Grant 51577088.

The authors are with the Jiangsu Key Laboratory of New Energy Generation and Power Conversion, College of Automation Engineering, Nanjing University of Aeronautics and Astronautics, Nanjing 211106, China (e-mail: liuhuawu@nuaa.edu.cn; xingyan@nuaa.edu.cn; huhaibing@nuaa.edu.cn).

Color versions of one or more of the figures in this letter are available online at http://ieeexplore.ieee.org.

Digital Object Identifier 10.1109/TPEL.2016.2564994

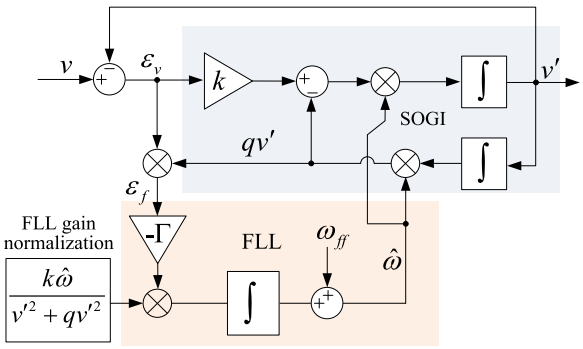

Fig. 1. Block diagram of the conventional SOGI-FLL [18].

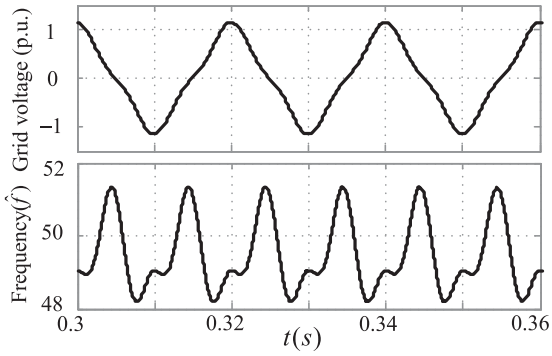

Fig. 2. Steady-state performance of the SOGI-FLL when the grid voltage is distorted with 15% third harmonic ($k = \sqrt{2}$ and $\Gamma = 160$).

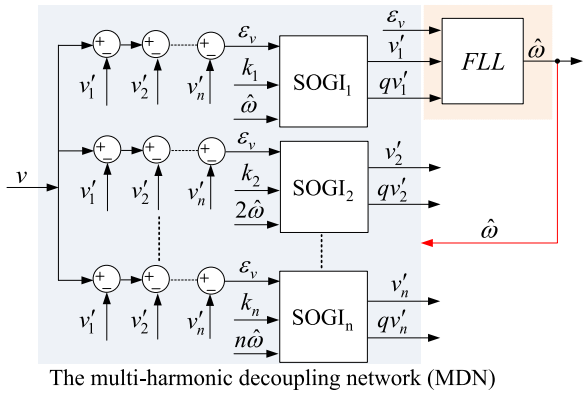

Fig. 3. Block diagram of the typical existing solution, MSOGI-FLL [14].

typical example is the MSOGI-FLL [14], [15] in Fig. 3. Each SOGI filter is tuned at one harmonic frequency, and they operate collaboratively to completely remove the unexpected harmonics. The MOSGI-FLL is an effective solution even under heavily distorted conditions. However, it suffers from the following drawbacks: 1) heavy computational load due to the multiple SOGI filters; 2) complex structure, which poses challenges on parameter tuning of the filtering gains (i.e., $k_1, k_2, \ldots, k_n$) and the FLL; and 3) compared with the conventional SOGI-FLL, dynamics of the MSOGI-FLL can be affected due to interactions

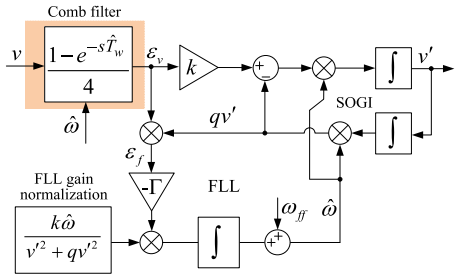

Fig. 4. Block diagram of the proposed FLL.

between SOGI filters, especially when their tuned frequencies are close to each other [6].

B. Proposed FLL With a Comb Filter

The basic concept of the MDN in the MSOGI-FLL is to first extract a specific harmonic component through one SOGI filter, and then the extracted harmonic signal is subtracted from the input grid signal to eliminate its influence on the FLL. This process introduces two purely imaginary *zeros* at the harmonic frequency in the transfer function from v'_1, qv'_1 to the input v (refer to Appendix A), and the introduced *zeros* provide zero gain to completely eliminate the corresponding harmonic. Inspired by this concept, a comb filter, which can introduce a cluster of *zeros* at harmonic frequencies, i.e., $s = jk\hat{\omega}(k = 0, \pm1, \pm2, \ldots)$, is proposed to be incorporated into the FLL:

$$F(s) = \frac{1 - e^{-sT_w}}{4} \tag{1}$$

where $\hat{T}_w$ is referred to as the window length, and is obtained through the estimated grid frequency $\hat{\omega}$, i.e., $\hat{T}_w = 2\pi/\hat{\omega}$. The proposed FLL is illustrated in Fig. 4.

Substituting $s = j\omega$ into $F(s)$, it can be obtained that

$$F(j\omega) = \frac{1}{2}\left|\sin(\omega\hat{T}_w/2)\right| \angle\left(\frac{\pi}{2} - \omega\hat{T}_w/2\right). \tag{2}$$

From (2), it can be seen that the comb filter provides zero gain at $f = n/\hat{T}_w (n = 0, 1, 2, \ldots)$, which indicates the harmonics with frequency of integer multiples of $\hat{f} = 1/\hat{T}_w$, including the dc, odd and even components, are completely blocked. To further evaluate the proposed method, transfer functions from the two in-quadrature signals v', qv', and the error signal ε_v, to the input grid voltage v, can be derived as

$$\begin{cases} D(s) = \dfrac{v'}{v}(s) = \dfrac{1 - e^{-s\hat{T}_w}}{4} \dfrac{k\hat{\omega}s}{s^2 + \hat{\omega}^2} \\ Q(s) = \dfrac{qv'}{v}(s) = \dfrac{1 - e^{-s\hat{T}_w}}{4} \dfrac{k\hat{\omega}^2}{s^2 + \hat{\omega}^2} \\ E(s) = \dfrac{\varepsilon_v}{v}(s) = \dfrac{1 - e^{-s\hat{T}_w}}{4} \end{cases} \tag{3}$$

where k is the filtering gain, and in order to ensure unity gain of $D(s), Q(s)$ at the fundamental frequency, it is set to $4/\pi$ (refer to Appendix B for details). Bode diagrams of (3) with $\hat{\omega} = 100\ \pi$ are plotted, and compared with the SOGI-FLL [18] of Fig. 1 and the MSOGI-FLL [14] of Fig 3. The results are demonstrated

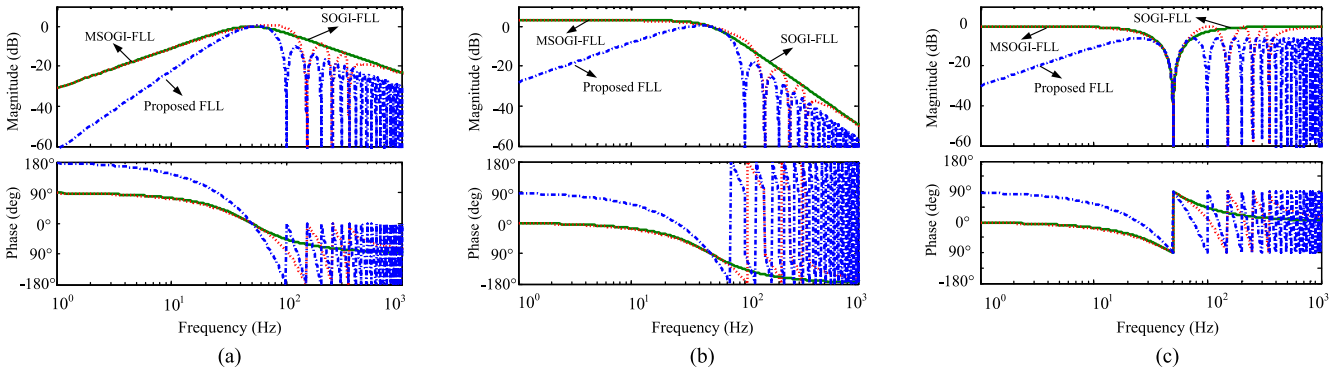

Fig. 5. Bode plots of the transfer functions, (a) $D(s)$, (b) $Q(s)$, (c) $E(s)$, of the proposed FLL, SOGI-FLL [18], and MSOGI-FLL [14].

in Fig. 1. Key parameters of SOGI-FLL and MSOGI-FLL are set according to the literatures [14], [18]. For SOGI, the filter gain k is $\sqrt{2}$ [18]. The MSOGI-FLL is tuned at the third, fifth, and seventh harmonic frequencies, and the parameters are $k_1 = \sqrt{2}, k_3 = \sqrt{2}/3, k_5 = \sqrt{2}/5, k_7 = \sqrt{2}/7$ [14]

$$\begin{cases} v'(t) = \dfrac{V\hat{\omega}\omega}{\pi(\omega^2-\hat{\omega}^2)}\left[\sin(\omega t)u(t) - \sin\omega(t-\hat{T}_w)u(t-\hat{T}_w)\right] \\ \qquad - \dfrac{V\hat{\omega}^2}{\pi(\omega^2-\hat{\omega}^2)}\left[\sin(\hat{\omega}t)u(t) - \sin(\hat{\omega}t)u(t-\hat{T}_w)\right] \\ qv'(t) = -\dfrac{V\hat{\omega}^2}{\pi(\omega^2-\hat{\omega}^2)}\left[\cos(\omega t)u(t) - \cos\omega(t-\hat{T}_w)u(t-\hat{T}_w)\right] \\ \qquad + \dfrac{V\hat{\omega}^2}{\pi(\omega^2-\hat{\omega}^2)}\left[\cos(\hat{\omega}t)u(t) - \cos(\hat{\omega}t)u(t-\hat{T}_w)\right]. \end{cases} \tag{4}$$

From Fig. 5, it can be seen that the SOGI-FLL exhibits poor attenuation ability especially for low-order harmonics. The MSOGI-FLL enhances the filtering characteristics by providing notches at the frequencies (i.e., third, fifth, and seventh), where the SOGI filters are tuned. The proposed FLL provides the best harmonic rejection abilities, and multiple notches centered at integer multiples of $\hat{f} = 1/\hat{T}_w$ are introduced to completely remove the harmonics. Besides, from (1) and Fig. 4, it can be seen that the comb filter features simple structure and low computational burden when compared with the multiple notch-filter-based FLLs [5], [11]–[13]. On the other hand, unlike these in-loop filters [7]–[11], which essentially work as low-pass filters and cannot be directly applied to the FLLs, the proposed FLL functions as a bandpass filter to accurately extract v', qv' as in Fig. 5. Moreover, as will be demonstrated in the next section, fast dynamics of the original SOGI-FLL are maintained in the proposed FLL.

III. Dynamic Analysis and Parameter Tuning of the Proposed FLL

In this section, dynamic analysis and parameter tuning of the proposed PLL are presented. It is shown that the incorporated comb filter will not deteriorate (and, can even slightly improve) the dynamic of the original SOGI-FLL. Since ANF-FLLs are highly nonlinear, the conventional analysis method based on bode plots (i.e., crossover frequency, phase margin, etc.) cannot be directly applied. Therefore, a simplified time-domain method

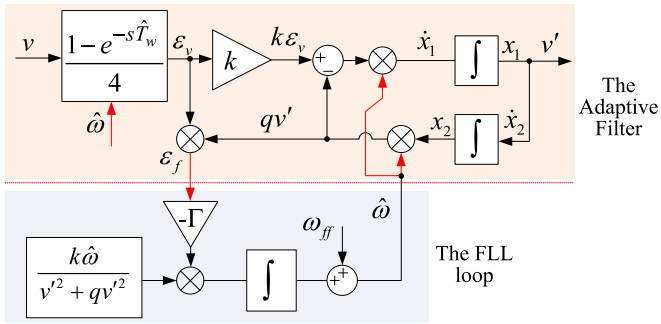

Fig. 6. Dynamic analysis of the proposed FLL.

is adopted. As shown in Fig. 6, the proposed FLL is spilt into two parts: the adaptive filter and the FLL loop, and they are analyzed separately.

A. Dynamic Analysis of the Adaptive Filter

Dynamic analysis of the adaptive filter is performed by disabling the FLL loop, and considering a given input $v = V\cos(\omega t)$ with $\omega \neq \hat{\omega}$, the transient outputs of v', qv' can be obtained from (3) as in (4) where $u(t)$ and $u(t-\hat{T}_w)$ are the unit step function. After one fundamental period $\hat{T}_w$, the second term in (4) becomes zero, and the settling time is only $\hat{T}_w$. The transient response time for the AF of the conventional SOGI-FLL under the same step sinusoidal input is, however, around 1.1 $\hat{T}_w$ [14], [18]. Besides, outputs of v', qv' in (4) exhibit "overdamping" properties and there is no amplitude overshoot. This further enhances the dynamics of the FLL loop, helping to reduce the frequency overshoot in transients. It is worth noticing here that the added comb filter modifies the control structure of the AF (note that in the original SOGI-FLL of Fig. 1, v' is feedback and subtracted from the input v while the subtraction is included by the comb filter in the proposed FLL), and the proposed FLL cannot be simply viewed as the comb filter in cascaded with the SOGI-FLL, which can be further shown by the AF transfer functions in (3) and those in [18].

B. Dynamic Analysis and Parameter Tuning of the FLL loop

In order for dynamic analysis and parameter (i.e., Γ) tuning of the FLL loop, a simplified system model is first derived

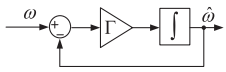

Fig. 7. Simplified model of the FLL loop.

following the same procedure in [11]. As shown in Fig. 6, the input to the FLL loop ε_f contains the frequency information, which, in steady state, can be described by (refer to Appendix C for details)

$$\bar{\varepsilon}_f \approx \frac{V^2}{k\hat{\omega}}(\hat{\omega}-\omega) \tag{5}$$

where V is the amplitude of the fundamental component. ω, $\hat{\omega}$ are the actual and estimated grid frequency. k is equal to $4/\pi$. Further, considering the gain normalization in Fig. 6, averaged dynamics of the FLL can be obtained as

$$\dot{\hat{\omega}} = -\Gamma\frac{k\hat{\omega}}{v'^2+qv'^2}\bar{\varepsilon}_f = -\Gamma(\hat{\omega}-\omega) \tag{6}$$

which gives the simplified model of FLL loop in Fig. 7. The obtained model is the same with that of the conventional SOGI-FLL [18] indicating that the incorporated comb filter will not deteriorate the FLL dynamics. The settling time of the FLL can be approximated by $t_s \approx 5/\Gamma$, and in this letter, $\Gamma$is set 160 to achieve a settling time of around 30 ms.

In practice, the FLL is realized in a discrete device, and discrete-time analysis/tuning is more accurate. Yet, it should be noted that the FLL dynamics is slow and its bandwidth (typically less than 50 Hz) is much lower than the sampling frequency (10 kHz in the letter). Therefore, the s-domain analysis/tuning can be directly transformed to the z-domain with pretty high accuracy.

IV. Experimental Results

The proposed FLL is applied to the single-phase grid, and it can be easily extended to the three-phase system based on the positive/negative calculation algorithms [14], [16]. During the experiments, a programmable ac source (Chroma 61503) is used to simulate the grid with 50 Hz nominal frequency, and the sampling frequency is fixed at 10 kHz. Frequency adaptiveness of the comb filter is realized through online adjustment of the window length $\hat{T}_w$ based on the first-order Lagrange interpolation approach [20]. The conventional SOGI-FLL [18] is also included for comparisons. The parameters are set at $k=\sqrt{2}$ [18] and $\Gamma = 160$.

Fig. 8 shows the steady-state experimental results of the proposed FLL under distorted grid conditions, where v_g is the input grid. v', qv' are the extracted fundamental and its orthogonal components, and $\tilde{f}$ is the estimated frequency. The grid voltage parameters are $V_1 = 1$ (p.u.), $V_0 = 0.1$ (p.u.) (dc component), $V_2 = 0.1$ (p.u.), $V_3 = 0.3$ (p.u.), $V_5 = V_7 = 0.1$ (p.u.), $V_{11} = 0.05$ (p.u.). It can be seen that the proposed FLL demonstrates excellent filtering capability, while the SOGI-FLL is severely affected by the grid harmonics.

Fig. 9 shows the dynamic experiments of the FLLs when the grid voltage undergoes a 10 Hz frequency step change and a 40° phase angle jump. It can be observed that the proposed FLL offers fast dynamics, i.e., around 30 ms for the 10 Hz frequency step and 35 ms for the 40° phase jump. The transient response of the proposed FLL is a little better, i.e., shorter settling time and smaller overshoot, than the conventional SOGI-FLL,

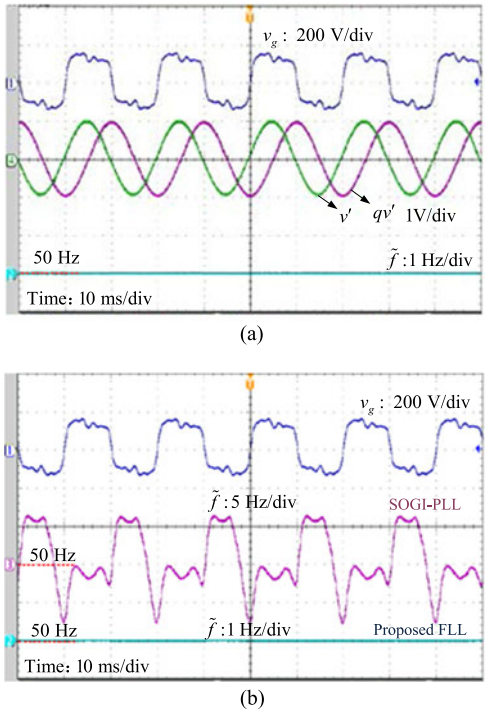

Fig. 8. Performance of the FLLs under distorted grid with dc component and harmonics.

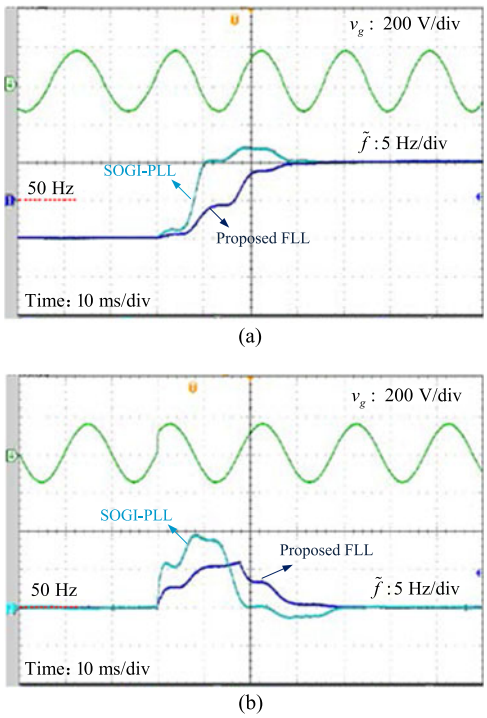

Fig. 9. Dynamic responses of the FLLs under (a) 10 Hz frequency step and (b) 40° phase angle jump.

TABLE I
BRIEF SIMULATION COMPARISONS OF THE ADVANCED PLLS/FLLS AND THE PROPOSED FLL

Aspects	Proposed FLL	SOGI-FLL [15]	MSOGI-FLL [11]	MAF-PLL with PID controller [7]	MAF-PLL with phase-lead compensator [9]
40° Phase angle jump					
2% Settling time	35 ms	42 ms	63 ms	40 ms	35.8 ms
Peak frequency error	6.1 Hz	9.8 Hz	5.1 Hz	16.4 Hz[1]	6.43 Hz
10 Hz frequency step					
2% Settling time	30 ms	35 ms	65 ms	41 ms	44.1 ms
Frequency overshoot	0 Hz	2.2 Hz	0.5 Hz	8.6 Hz[1]	0.41 Hz
Harmonic rejection ability	Excellent (completely eliminating DC, odd and even harmonics)	Poor (attenuating but not eliminating harmonics)	Good (completely eliminating selective harmonics)	Good[2] (completely eliminating odd harmonics)	Good[2] (completely eliminating odd harmonics)
Complexity and computational burden	Low	Low	High	Low	Low

[1]The peak frequency error under phase-angle jump test and the frequency overshoot under the frequency step test can be significantly reduced by considering the output signal of the integrator of the loop filter as the estimated frequency.
[2]In these PLLs, the window length (T_w) of MAF is set to be 0.01 s. T_w can be increased to 0.02 s to eliminate both odd and even harmonics, but at the cost of increased response time [7].

which is in agreement with the theoretical analysis (refer to (4) in Section III).

In order to evaluate the performances of the proposed FLL, some of the state-of-art advanced PLLs/FLLs, the MSOGI-FLL [14], MAF-PLL with PID controller [7], and MAF-PLL with phase-lead compensator [12] are simulated and compared in Simulink/MATLAB under the same test cases. Parameter tuning of the FLLs/PLLs are made according to the corresponding literatures [7], [12], [14], [18]. Table I presents the simulation results, from which it can be seen that the proposed FLL features low computational load, excellent harmonic rejection ability, and the fastest dynamics.

V. CONCLUSION

An enhanced FLL for adverse grid conditions is proposed through incorporating a comb filter. Compared to the multiple notch-filter-based FLLs, the proposed FLL has the advantage of load computational load and can completely eliminate the dc component, odd and even harmonics without deteriorating the FLL dynamics. Experimental results show that the proposed FLL exhibit excellent performances even under heavily distorted grid conditions, and the settling time for a frequency step change of 10 Hz and for a phase jump of 40° is around 30 and 35 ms.

APPENDIX

A. Analysis of the MOSGI-FLL

Here, influences of inserting the MDN in the MOSGI-FLL [14] are analyzed. Referring to [14] and Fig. 3, the transfer function to extract v'_1 in the MOSGI-FLL is described by

$$\frac{v'_1}{v}(s) = D_1(s)\underbrace{\prod_{k=2}^{n}\left(\frac{1-D_k(s)}{1-D_1(s)D_k(s)}\right)}_{M_k(s)} \tag{A.1}$$

where $D_1(s)$ is the transfer function from v'_1 to the input grid signal v in the original SOGI-FLL. Therefore, $M_k(s)$ in (A.1) actually represents the effects of introducing the kth-SOGI filter, i.e., the SOGI_k in Fig. 3, and $M_k(s)$ can be obtained as

$$M_k(s) = \left[s^2 + (k\hat{\omega})^2\right]\underbrace{\frac{1}{s^2 + k_k\hat{\omega}s + (k\hat{\omega})^2}\cdot\frac{1}{1-D_1(s)D_k(s)}}_{N_k(s)} \tag{A.2}$$

where k_k is the filtering gain of the kth-SOGI filter. From (A.2), it can be seen that two purely imaginary *zeros* at $s = \pm jk\hat{\omega}$ are introduced. The zeros help to completely eliminate the kth harmonic from the grid voltage, and the remaining $N_k(s)$ might affect the system dynamics.

B. Derivation of the Filtering Gain

Transfer function of $D(s)$ in (3) is taken as an example to obtain the filtering gain k, and applying *L'Hôspital's Rule for Complex-value Functions* yields

$$D(s)\,|_{s=j\hat{\omega}} = \lim_{s\to j\hat{\omega}} D(s) = \lim_{s\to j\hat{\omega}}\frac{[(1-e^{-s\hat{T}_w})k\hat{\omega}s]'}{[4(s^2+\hat{\omega}^2)]'} = \frac{k\pi}{4}. \tag{B.1}$$

Based on (B.1) and setting $D(s)|_{s=j\hat{\omega}} = 1$, it is derived that $k = 4/\pi$.

C. Derivation of the Simplified Model of the FLL

Here, the steady-state output of frequency error ε_f is derived. From Fig. 6, the following state equations can be obtained as

$$\begin{cases} \dot{x}_1(t) = -\hat{\omega}^2 x_2(t) + \frac{k\hat{\omega}}{4}[v(t) - v(t-\hat{T}_w)] \\ \dot{x}_2(t) = x_1(t) \\ \varepsilon_v(t) = \frac{1}{4}[v(t) - v(t-\hat{T}_w)]. \end{cases} \tag{C.1}$$

Combining the three equations in (C.1), it can be easily derived that $\varepsilon_v(t) = (1/k\hat{\omega})[\dot{x}_1(t) + \hat{\omega}^2 x_2(t)]$. Further, the steady-state equation of $\dot{\bar{x}}_1 = -\omega^2\bar{x}_2$ holds even when $\omega \neq \hat{\omega}$ [16], [18]. Therefore, the steady-state output of ε_f is

$$\bar{\varepsilon}_f = \hat{\omega}\bar{\varepsilon}_v\bar{x}_2 = \frac{\bar{x}_2^2}{k}(\hat{\omega}^2 - \omega^2). \tag{C.2}$$

The steady-state output of x_2, i.e., $qv'/\hat{\omega}$, for a given sinusoidal input can be derived from (4) as

$$\bar{x}_2 = \frac{qv'}{\hat{\omega}} = -\frac{2}{\pi}\frac{\hat{\omega}V}{\omega^2-\hat{\omega}^2}\sin\left(\frac{\pi\omega - \pi\hat{\omega}}{\hat{\omega}}\right)\sin\left(\omega t + \frac{\pi\omega}{\hat{\omega}}\right). \tag{C.3}$$

Averagely $\omega \approx \hat{\omega}$. Thus, $\sin[(\pi\omega - \pi\hat{\omega})/\hat{\omega}] \approx (\pi\omega - \pi\hat{\omega})/\hat{\omega}$, and $\bar{x}_2^2$ is given by

$$\bar{x}_2^2 \approx \left[-\frac{2}{\pi}\frac{\hat{\omega}V}{\omega^2-\hat{\omega}^2}\frac{\pi\omega-\pi\hat{\omega}}{\hat{\omega}}\sin\left(\omega t+\frac{\pi\omega}{\hat{\omega}}\right)\right]^2 = \frac{2V^2}{(\omega+\hat{\omega})^2}\left[1-\cos\left(2\omega t+\frac{2\pi\omega}{\hat{\omega}}\right)\right]. \quad \text{(C.4)}$$

Neglecting the ac term, and taking (C.4) into (C.2) yields $\bar{\varepsilon}_f = 2V^2/[k(\hat{\omega}+\omega)](\hat{\omega}-\omega) \approx V^2/(k\hat{\omega})(\hat{\omega}-\omega)$.

REFERENCES

[1] P. Xiao, K. A. Corzine, and G. K. Venayagamoorthy, "Multiple reference frame-based control of three-phase PWM boost rectifiers under unbalanced and distorted input conditions," *IEEE Trans. Power Electron.*, vol. 23, no. 4, pp. 2006–2017, Jul. 2008.

[2] X. Guo, W. Wu, and Z. Chen, "Multiple-complex coefficient-filter-based phase-locked loop and synchronization technique for three-phase grid-interfaced converters in distributed utility networks," *IEEE Trans. Ind. Electron.*, vol. 58, no. 4, pp. 1194–1204, Apr. 2011.

[3] L. Hadjidemetriou, E. Kyriakides, and F. Blaabjerg, "A robust synchronization to enhance the power quality of renewable energy systems," *IEEE Trans. Ind. Electron.*, vol. 62, no. 8, pp. 4858–4868, Aug. 2015.

[4] G. De Donato, G. Scelba, G. Borocci, F. G. Capponi, and G . Scarcella, "Fault-decoupled instantaneous frequency and phase angle estimation for three-phase grid-connected inverters," *IEEE Trans. Power Electron.*, vol. 31, no. 4, pp. 2880–2889, Jul. 2016.

[5] S. G. Jorge, C. A. Busada, and J. A. Solsona, "Frequency adaptive discrete filter for grid synchronization under distorted voltages," *IEEE Trans. Power Electron.*, vol. 27, no. 8, pp. 3584–3594, Aug. 2012.

[6] S. Golestan, M. Monfared, and F. D. Freijedo, "Design-oriented study of advanced synchronous reference frame phase-locked loops," *IEEE Trans. Power Electron.*, vol. 28, no. 2, pp. 765–778, Feb. 2013.

[7] S. Golestan, M. Ramezani, J. M. Guerrero, F. D. Freijedo, and M. Monfared, "Moving average filter based phase-locked loops: Performance analysis and design guidelines," *IEEE Trans. Power Electron.*, vol. 29, no. 6, pp. 2750–2763, Jun. 2014.

[8] M. A. Perez, J. R. Espinoza, L. A. Moran, M. A. Torres, and E. A. Araya, "A robust phase-locked loop algorithm to synchronize static-power converters with polluted AC systems," *IEEE Trans. Ind. Electron.*, vol. 55, no. 5, pp. 2185–2192, May 2008.

[9] Y. F. Wang and Y. W. Li, "Grid synchronization PLL based on cascaded delayed signal cancellation," *IEEE Trans. Power Electron.*, vol. 26, no. 7, pp. 1987–1997, Jul. 2011.

[10] S. Golestan, M. Ramezani, J. M. Guerrero, and M. Monfared, "DQ-frame cascaded delayed signal cancellation-based PLL: Analysis, design, and comparison with moving average filter-based PLL," *IEEE Trans. Power Electron.*, vol. 30, no. 3, pp. 1618–1632, Mar. 2015.

[11] M. Rashed, C. Klumpner, and G. Asher, "Repetitive and resonant control for a single-phase grid-connected hybrid cascaded multilevel converter," *IEEE Trans. Power Electron.*, vol. 28, no. 5, pp. 2224–2234, May 2013.

[12] S. Golestan, J. M. Guerrero, and A. M. Abusorrah, "MAF-PLL with phase-lead compensator," *IEEE Trans. Ind. Electron.*, vol. 62, no. 6, pp. 3691–3695, Jun. 2015.

[13] S. Golestan, J. M. Guerrero, A. M. Abusorrah, and Y. Al-Turki, "Hybrid synchronous/stationary reference-frame-filtering-based PLL," *IEEE Trans. Ind. Electron.*, vol. 62, no. 8, pp. 5018–5022, Aug. 2015.

[14] P. Rodriguez, A. Luna, I. Etxeberria, R. Mujal, R. Teodorescu, and F. Blaabjerg, "Multi-resonant frequency-locked loop for grid synchronization of power converters under distorted grid conditions," *IEEE Trans. Ind. Electron.*, vol. 58, no. 1, pp. 127–138, Jan. 2011.

[15] S. Vazquez, J. A. Sanchez, M. R. Reyes, J. I. Leon, and J. M. Carrasco, "Adaptive vectorial filter for grid synchronization of power converters under unbalanced and/or distorted grid conditions," *IEEE Trans. Ind. Electron.*, vol. 61, no. 3, pp. 1355–1367, Mar. 2014.

[16] D. Yazdani, M. Mojiri, A. Bakhshai, and G. Joos, "A fast and accurate synchronization technique for extraction of symmetrical components," *IEEE Trans. Power Electron.*, vol. 24, no. 3, pp. 674–684, Mar. 2009.

[17] G. Yin, L. Guo, and X. Li, "An amplitude adaptive notch filter for grid signal processing," *IEEE Trans. Power Electron.*, vol. 28, no. 6, pp. 2638–2641, Jun. 2013.

[18] P. Rodríguez, A. Luna, R. S. Muñoz-Aguilar, I. Etxeberria-Otadui, R. Teodorescu, and F. Blaabjerg, "A stationary reference frame grid synchronization system for three-phase grid-connected power converters under adverse grid conditions," *IEEE Trans. Power Electron.*, vol. 27, no. 1, pp. 99–112, Jan. 2012.

[19] J. Matas, M. Castilla, J. Miret, L. Garcia De Vicuna, and R. Guzman, "An adaptive prefiltering method to improve the speed/accuracy tradeoff of voltage sequence detection methods under adverse grid conditions," *IEEE Trans. Ind. Electron.*, vol. 61, no. 5, pp. 2139–2151, May 2014.

[20] G. Escobar, M. H-Gomez, A. A. V-Fernandez, M. J. Lopez-Sanchez, and G. A. Catzin-Contreras, "Implementation of a 6n $\pm$ 1 repetitive controller subject to fractional delays," *IEEE Trans. Ind. Electron.*, vol. 62, no. 1, pp. 444–452, Jan. 2015.